The Rosseland Mean Opacity of a Composite Material at High Temperatures

T. J. Orzechowski *H. N. Kornblum* *R. J. Wallace*

M. D. Rosen *L. J. Suter* *L. J. Porter**

A. R. Thiessen

Introduction

The indirect-drive approach[1] to inertial confinement fusion (ICF)[2] relies on thermal x-ray radiation to drive the implosion of the fuel capsule. This radiation is generated by the interaction of intense beams—either lasers[3] or particles[4]—with the interior wall of a high-Z cavity or hohlraum. The radiation is usually described by a blackbody spectrum with a temperature of about 250 eV. This high-temperature radiation not only drives the fuel pellet compression, but it also heats and ablates the hohlraum wall. In this article, we describe a method for making the hohlraum wall more opaque to the drive radiation. This leads to lower losses and more energy available to implode the fuel.

The interaction of the radiation with the hohlraum wall is characterized by multiple absorption and reemission of the x rays.[5–7] The ratio of the reemitted flux to the incident flux is referred to as the albedo, α. The efficiency with which the radiation couples to the capsule depends on the albedo; increasing the albedo improves the drive efficiency. The incident flux is the sum of the reemitted flux plus the x-ray flux lost to the wall. The flux lost to the wall propagates through the wall in the form of a diffusive ablative heat wave.[8] Figure 1 shows how radiation propagates through the high-Z wall material. The details of this radiation flow will be discussed in the next section. The rate of diffusion is (approximately) inversely proportional to the square root of the Rosseland mean opacity,[9] which is used to describe radiation transport in optically thick materials when the matter and radiation are in thermodynamic equilibrium. It is defined as a weighted harmonic mean of the frequency-dependent opacity:

$$\frac{1}{\kappa_R} \equiv \frac{\int_0^\infty \kappa_\nu^{-1} \frac{\partial B_\nu}{\partial T} d\nu}{\int_0^\infty \frac{\partial B_\nu}{\partial T} d\nu} \quad . \tag{1}$$

Here, κ_R is the Rosseland mean opacity, κ_ν is the frequency-dependent opacity, B_ν is the blackbody spectrum, and T is the radiation and material temperature. This mean opacity is dominated by the minima in the frequency-dependent opacity. Increasing the Rosseland mean opacity reduces the radiation energy lost to the walls, thereby increasing the drive temperature and improving the coupling efficiency of the radiation to the fuel pellet for a given laser power (and x-ray conversion efficiency).

Typically we use pure Au hohlraums heated to ~250 eV. Figure 1 shows a frequency-dependent opacity for Au at a density and temperature relevant to these experiments. This opacity was calculated using a very simple average atom model[10] for Au at 1.0 g/cm^3 and a temperature of 250 eV. There are significant windows in the opacity at energies around the peak of the blackbody spectrum. The gross structure of the opacity in Figure 2(a) is dominated by the bound-free (photoelectric) absorption coefficient; the sharp increases in opacity correspond to the photoionization of the atomic shells (K, L, M…). Figure 2(a) also shows the weighting function $\partial B_\nu / \partial T$ used in the definition of the Rosseland mean opacity for a 250-eV blackbody distribution. The peak of the weighting function is fairly broad (~1 keV FWHM), and it occurs at about 1 keV, which is near the minimum in the opacity between the N- and O-band absorption edges. To improve the efficiency of the hohlraum, we need to

* Sandia National Laboratories, Albuquerque, New Mexico

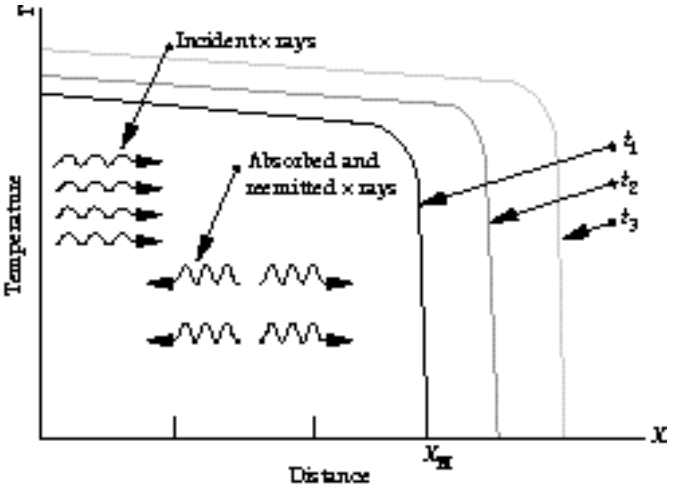

FIGURE 1. Schematic of radiation diffusion (Marshak wave propagation) into high-Z material. Blackbody radiation is incident on the material at $X = 0$. The front of the heat wave at any given time t is indicated by X_M. In this schematic, the temperature is a weakly increasing function of time. (70-00-0197-0143pb01)

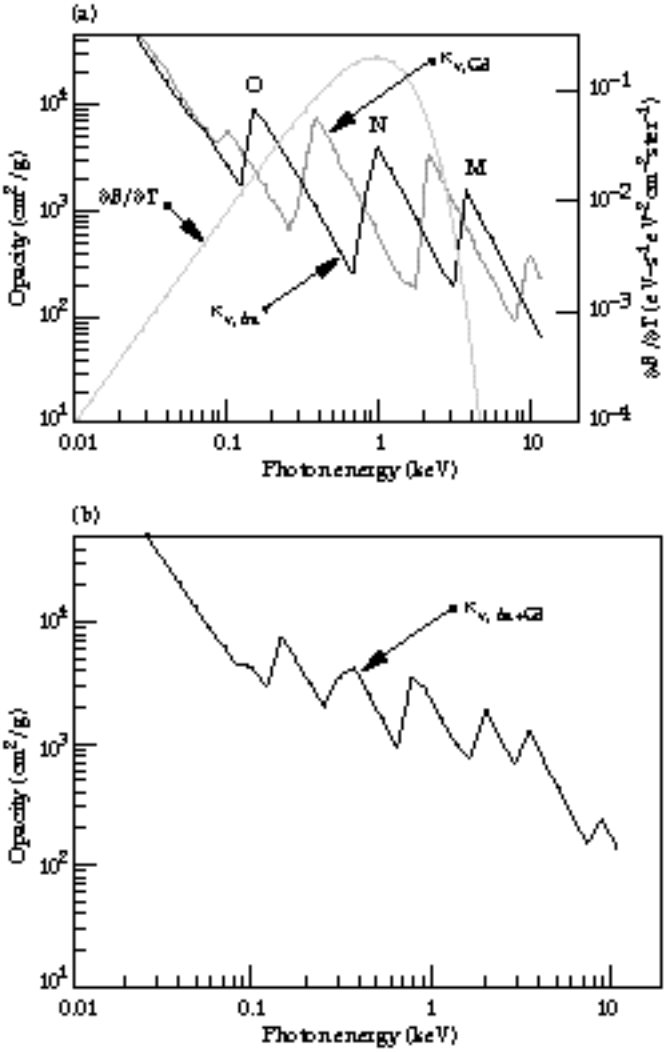

FIGURE 2. (a)Frequency (energy)-dependent opacity of Au and Gd. Also shown is the weighting function ($\partial B/\partial T$) used in the definition of the Rosseland mean opacity corresponding to a 250-eV Planckian distribution. (b) Frequency (energy)-dependent opacity of a 50:50 mixture of Au and Gd at a density of 1 g/cm^3 and a temperature of 250 eV. (70-00-0197-0144pb01)

blend-in materials whose high-opacity regions complement the low-opacity regions of the original material.[11] Figure 2(a) also shows the calculated frequency-dependent opacity for gadolinium at T = 250 eV at a density of 1.0 g/cm^3. Gd was chosen because its high-opacity regions occur around the same frequency as the holes in the Au opacity. For the frequency-dependent opacities shown here, the Rosseland mean opacity for Au is 823 cm^2/g and 455 cm^2/g for Gd. In a properly designed material containing both atoms, the radiation samples the combined opacity of both materials resulting in a higher Rosseland mean opacity. Using the opacity model employed in generating Figure 2(a), the Rosseland mean opacity of a 50:50 mixture of gold and gadolinium, with density 1 g/cm^3 and temperature 250 eV, is 1390 cm^2/g. The frequency-dependent opacity of this composite material is shown in Figure 2(b). A more sophisticated opacity model, XSN,[12] wherein bound-bound transitions play a more central role in determining opacity, would give κ_R = 1500 cm^2/g for Au, 1300 cm^2/g for Gd, and 2500 cm^2/g for the 50:50 Au/Gd mixture at the same density and temperature.

Analytic Model of Radiation Flow through High-Z Material

In order to determine the Rosseland mean opacity of a material, we measure the propagation time of a radiation heat wave (also referred to as a Marshak wave) through a well characterized sample of that material and compare the measurement to analytic[13–15] and numerical solutions. The nonlinear diffusion equation that governs the Marshak wave behavior involves the specific energy density and the Rosseland mean opacity of the material. For the experiments discussed here, it can approximately be written as:

$$\frac{\partial}{\partial t}(\rho\varepsilon) = \frac{\partial}{\partial x}\left(\frac{4\sigma}{3\rho\kappa_R}\frac{\partial}{\partial x}T^4\right), \qquad (2)$$

where ρ is the material density, ε is the specific energy density of the material, and σ is the Stefan-Boltzmann constant. Using the XSN opacity model, the Rosseland mean opacity for Au in the temperature range of 100 to 300 eV is found to scale as $\kappa_R = \kappa_0 \rho^{0.33} T^{-1}$, where κ_R is in

cm^2/g, κ_0 is 3500 when ρ is in g/cm^3, and T is in heV (10^2 eV). The energy density of the material is approximated as $\varepsilon \approx \varepsilon_0 T^{1.5}$. With these analytic models for κ_R and ε, the self-similar solution for the diffusion equation gives the energy lost to the wall and the position of the Marshak wave front as a function of time and temperature:[6]

$$E_w \quad T^{3.0} t^{0.62} \kappa_0^{-0.4} \tag{3}$$

$$\rho X_M \quad T^{1.7} t^{0.55} \kappa_0^{-0.45} \quad . \tag{4}$$

These solutions were derived for a constant temperature. In a more general case, the boundary temperature itself can vary in time, thus changing the temporal dependence of E_w and ρX_M. For example, in the case of a constant absorbed x-ray flux on the wall, $\dot{E}_w = \text{const}(\ t^0)$, and from Eq. (3), we would have the temperature scaling as $T \quad t^{0.12}$. In this case, the position of the Marshak wave would scale as $t^{0.78}$. This is the sort of behavior one would expect for a constant laser power and a constant x-ray conversion efficiency. In fact, the x-ray conversion efficiency increases slowly in time. We will assume that $\eta_{c.e.} \quad t^{0.2}$, although measurements[16] from Au disks indicate that the conversion efficiency could be significantly higher ($\eta_{c.e.} \quad t^{0.4}$). Using this temporal behavior for the x-ray flux (and hence wall loss), we find the temperature to scale as $t^{0.18}$ and the Marshak wave position to scale almost linearly with time for constant laser power:

$$\rho X_M \quad t^{0.9} \kappa_0^{-0.45} \quad . \tag{5}$$

The time dependence of the Marshak wave position is very close to that observed experimentally[14] for Au foils of varying thickness exposed to the same hohlraum drive in these experiments ($\rho X_M \quad t$). We will also see below that this temporal dependence of the hohlraum temperature is close to that observed experimentally. Therefore, this model is probably the best representation of the experiment described here.

Measurement of Radiation Flow through High-Z Material

To measure the propagation of the heat wave through a given material, we expose the sample to the near Planckian radiation distribution generated inside a standard Nova hohlraum.[17] The sample materials are attached to the side of the hohlraum wall (Figure 3, top). Figure 3 (bottom) is a photograph of an actual sample patch on the side of the hohlraum. The standard Nova hohlraum consists of a 2700-μm-long-cylindrical cavity with a diameter of 1600 μm. The laser entrance holes (LEHs) on the ends of the hohlraum are 800 μm in diameter. The Nova laser beams, five from each end,

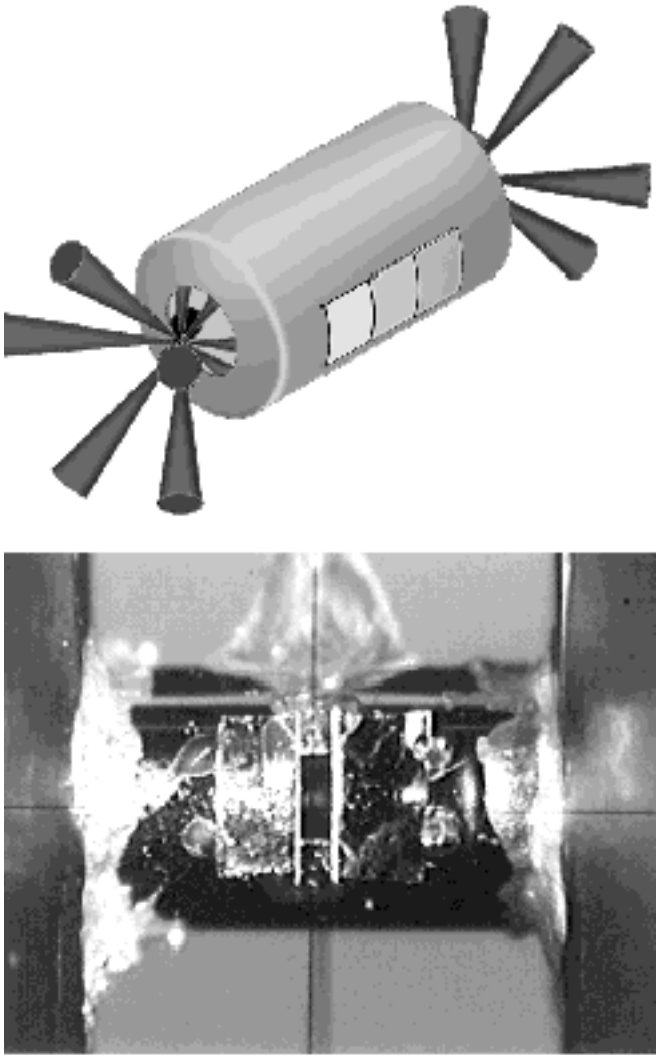

FIGURE 3. Schematic of hohlraum showing laser illumination scheme and sample package mounted on side of hohlraum (top); photograph of foils mounted on hohlraum (bottom). The region between the foils looks directly into the hohlraum and serves as a temporal fiducial. (70-00-0197-0145pb02)

enter the hohlraum through the LEHs and strike the inside of the hohlraum at 40° to the surface normal. The laser beams illuminate an annular region that is centered about 900 μm from the hohlraum midplane on each end of the hohlraum. For the experiments described here, the total laser energy is about 27 kJ, and the laser pulse duration is 1 ns. The five beams on each end intersect in the LEH and are focused 1000 μm in front of the LEH. The laser beam illumination on the hohlraum wall is roughly a 400-μm-×-600-μm ellipse. Thus the average laser intensity on the wall is about 10^{15} W/cm^2.

The hohlraum wall temperature is monitored with an absolutely calibrated multiple-channel soft x-ray spectrometer, DANTE.[18] This diagnostic views a portion of the interior hohlraum wall through a small hole in the hohlraum. Care is taken that DANTE does not view a

laser spot. In Figure 4, we show the temporal profile of the total laser power and the hohlraum temperature. The laser pulse rises rather sharply (~100 ps) and exhibits a small oscillation (±5%) during the "flat-top" region of the pulse. The corresponding hohlraum temperature rises more slowly, reaching a temperature of about 200 eV at 300 ps. Beyond this point, the hohlraum temperature rises more slowly with time ($\sim t^{0.15}$) during the nominal constant laser power. This is characteristic of the Marshak wave behavior in a material absorbing a constant flux as opposed to a material at constant temperature. The test sample package covers a 600-μm-high, 1200-μm-long slot that is cut in the hohlraum wall and is centered about the hohlraum midplane (see Figure 3). Various test materials cover portions of this slot with one section left uncovered to provide a fiducial signal at $t = 0$ (the beginning of the drive pulse). The sample package usually contains a pure Au sample and a sample of the mixture. The fiducial is located in the center and the burnthrough foils are mounted on either side of it to mitigate any possible effects of hohlraum temperature nonuniformity in the axial direction (i. e., higher hohlraum temperature closer to the laser spots). The radiation inside the hohlraum drives the Marshak wave into the material. Sample thicknesses are usually on the order of one to a few microns so that the radiation propagates through the sample before the drive (i. e., the laser beams) turns off.

In the measurements described here, we investigate the transport of the thermal wave through pure Au foils and Au/Gd mixtures. Two methods of fabricating the mixture are to cosputter the elements resulting in an amorphous material of Au/Gd, or to alternate layers of the constituent elements. A Au/Gd foil that was fabricated by cosputtering the Au and Gd atoms onto a substrate was found to be unacceptable because the internal stresses generated by this fabrication technique resulted in an extremely fragile material.

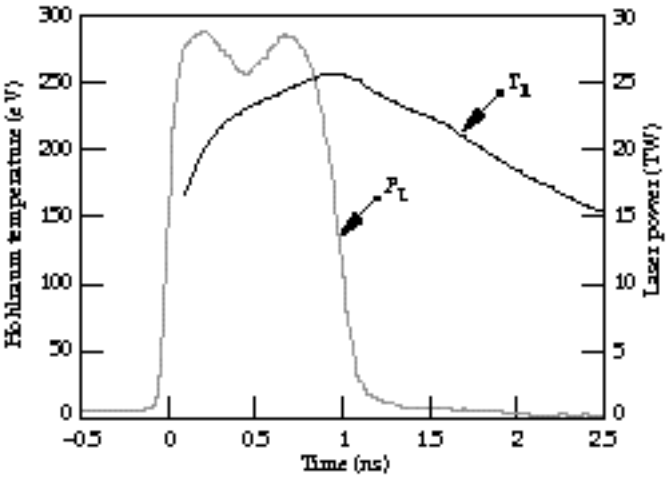

FIGURE 4. Typical 1-ns "square" laser pulse used to drive the hohlraum and the corresponding hohlraum temperature measured with DANTE and albedo corrected. (70-00-0197-0146pb01)

In the latter method of fabrication, the areal density of each layer must be optically thin to the radiation, so that the radiation samples both elements simultaneously and averages over the opacity of two elements. In this experiment, the Au/Gd samples are formed by depositing alternate layers of the two elements on a substrate, which is later removed to provide a free standing sample. Two different samples (of the multilayer variety) corresponding to different atomic fractions of Au and Gd were fabricated. One composite comprises 200 layer pairs of Au and Gd. The thickness of each Au layer is 75 Å, and the thickness of each Gd layer is 75 Å. This sample is 33% Gd and 67% Au by atom. The overall thickness is 2.22 μm, and the areal density of this sample is equivalent to 1.6 μm of Au (i. e., 3.15 mg/cm^2). The second sample comprises 146 layer pairs; the thickness of each Au layer is 35 Å, and the thickness of each Gd layer is 116 Å. In this case, the sample is 67% Gd and 33% Au. The overall thickness of this second sample is 3.02 μm, again corresponding to an equivalent areal mass of Au of 3.15 mg/cm^2. In either of these samples, the individual thickness of each layer of either the Au or the Gd is much less than the range of a photon (100–1000 eV) in these materials. For example, the cold opacity of Au to x rays between 100 and 1000 eV is between 0.5 and 1.5×10^4 cm^2/g. For solid density, then, the range of a photon is $(\kappa\rho)^{-1}$ or about 1000 Å, which is much larger than the typical layer thickness (~10^2 Å) and much less than the typical sample thickness (~10^4 Å).

The thermal radiation corresponding to the hohlraum drive is monitored as a function of time as it burns through the different foils using a streaked x-ray imager (SXI). The SXI images the foil in one direction using a 20-μm-wide imaging slit. The image is dispersed with a transmission grating oriented perpendicular to the imaging slit, and the energy at which we monitor the burnthrough is determined with an offset aperture located behind the transmission grating. All of the data discussed here corresponds to 225-eV radiation. The one-dimensional image is monitored with an x-ray streak camera. Figure 5 shows the streaked image for a sample patch mounted on the side of a hohlraum. The corresponding lineouts of the image (fiducial, pure Au foil and Au/Gd composite foil) are also shown. Figure 5 shows that the radiation burns through the composite foil about 100 ps after it burns through the pure Au foil.

To determine the ratio of the mixture's Rosseland mean opacity to that of Au, we used the results of self-similar solutions [Eq. (5)] and assumed that the two foils are exposed to the same temperature. Independent measurements on the uniformity of the temperature in the region of the test patch indicated that the hohlraum temperature is uniform to within

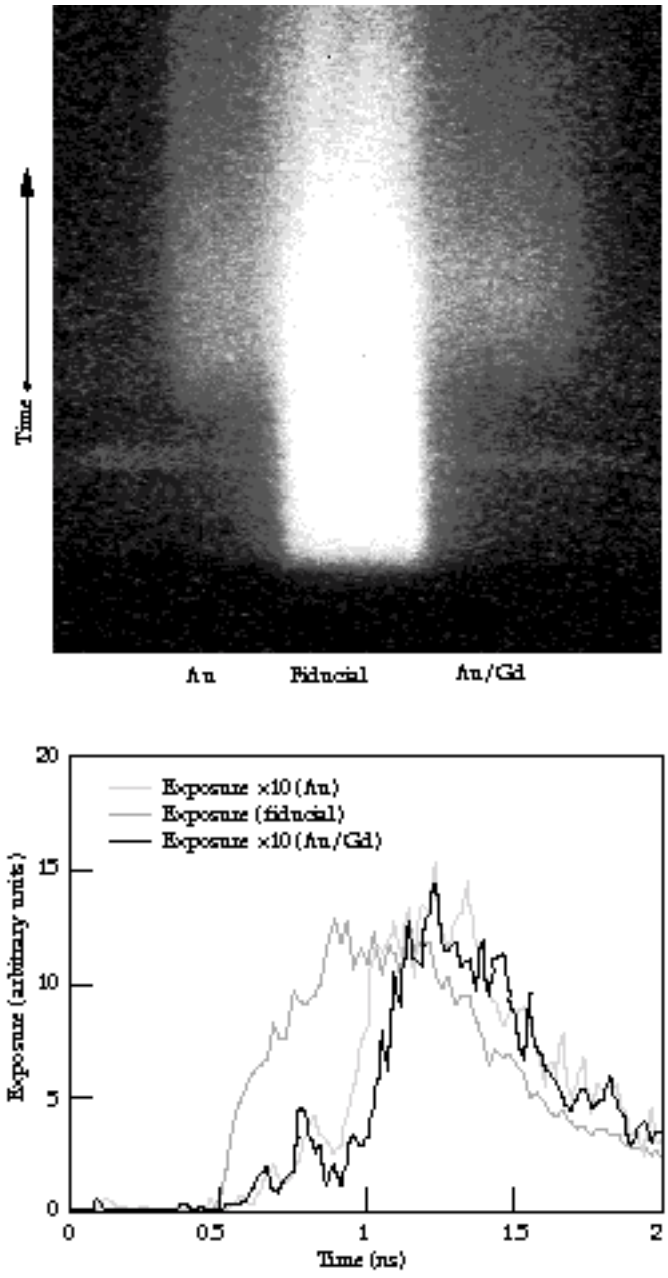

FIGURE 5. Streaked image of test-sample patch monitored at 225 eV (top). The fiducial signal is in the center of the image; the radiation burning through the pure Au sample is on the left of the fiducial, while the radiation burning through the Au/Gd composite sample is on the right. Lineouts of the three sections of the streaked image (bottom). The radiation burns through the Au/Gd composite about 100 ps after it burns through the equivalent areal mass of Au. (70-00-0197-0147pb01)

the accuracy of the measurement. The ratio of the Rosseland mean opacities then depends on the ratio of the burnthrough times squared and on the ratio of the areal masses of the foils to the 2.2 power. The foils were fabricated so that this latter quantity is nominally one, but the exact values were used in determining the ratio of opacities. Figure 6 shows the ratio of the Au/Gd foil's Rosseland mean opacities to that of Au for the two different concentrations of Gd. The errors associated with the measurement correspond to uncertainties in the streak camera sweep speed (±15 ps) and in errors in determining the precise thickness of the foils (±250 Å). In addition, the measured concentration of Gd is accurate to about ±5%. Figure 6 also shows the calculated Rosseland mean opacity of the Au/Gd mixture as a function of Gd concentration. For these calculations, we used the XSN opacity model and assumed a temperature of 250 eV and a density of 1.0 g/cm^3. The calculations were done for seven different Gd concentrations ranging from 0% to 100%; the solid line is a fit to these seven calculated points. These calculations indicate that the maximum improvement in opacity corresponds to a 50:50 mixture of Au and Gd. The overall improvement in the opacity (over that of pure Au at the same temperature and density) is a factor of 1.7. This curve is normalized to the Rosseland mean opacity of Au at 1.0 g/cm^3 at temperature of 250 eV (κ_R[Au]) = 1500 cm^2/g). The opacity of Gd at this temperature and density is 1300 cm^2/g. An independent series of experiments measured Marshak wave propagation through different thicknesses of Au foil (1–3 μm) and monitored the radiation at two different energies (225 and 550 eV).[14] In these experiments, the hohlraum temperatures were 250 to 265 eV, and they validated the XSN opacity model to within 20% for Au at these temperatures. We indicate the results of those experiments by the datum at the pure Au end of the curve (fraction Gd = 0%).

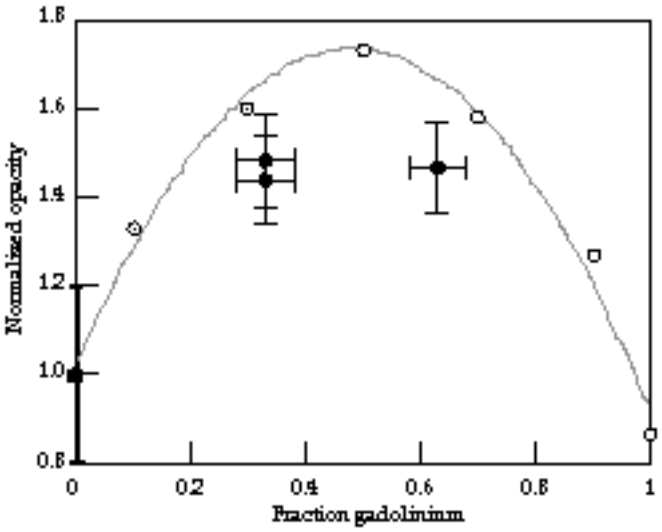

FIGURE 6. Rosseland mean opacity of a Au/Gd composite normalized to that of pure Au at a temperature of 250 eV and a density of 1 g/cm^3. The open points correspond to the results of XSN calculations, and the solid line is a quadratic fit to those points. The solid points show the normalized opacity of the measurements as determined using Eq. (5). The datum at zero concentration of Gd corresponds to earlier work that verified the XSN opacity model. (70-00-0197-0148pb01)

The analytic models yield insight into the physical processes that govern the behavior of the Marshak wave propagation and illustrate its sensitivity to the various parameters that affect it (κ_R, T, etc.). However, the real situation is quite complicated. For example, the absorbed laser power may not be constant in time because of parametric instabilities such as SRS, or hohlraum conversion efficiency may behave differently from "disk" conversion efficiency. Furthermore, the opacity calculation in Figure 6 represents one specific density and temperature. In reality, the experiment samples a range of densities and temperatures. In view of the relative simplicity of the model to the actual time dependent phenomenon, the model is remarkably accurate in that the measurements as interpreted by the model are only about 10 to 12% lower than the XSN calculation. Perhaps an even more sophisticated treatment of bound-bound transitions than that XSN employs would account for the discrepancy. The most accurate way of determining the opacity of the composite is to simulate the experiment with a rad-hydro code. Initial LASNEX calculations monitoring a 250-eV photon energy channel yield a burnthrough time in a 2:1 Au/Gd mixture that is 1.3 times longer than that in an equivalent areal mass of pure Au. The measured burnthrough time (at 225 eV) is 1.2 times longer. Similarly, the simulation gives a burnthrough time that is 1.25 times longer than that in an equivalent areal mass of pure Au for a 1:2 Au/Gd mixture while the measured burnthrough time is 1.3 times longer.

Conclusion

By combining the appropriate elements, we have demonstrated that we can produce a composite whose Rosseland mean opacity is higher than that of either of the constituents at a given temperature and density. The elements must be chosen so that the high-opacity regions (in photon energy) of one element overlap with the low-opacity regions of the other. Because the composites have a higher reemission coefficient to the incident radiation, less energy is lost to the wall. For example, in the scale-1 hohlraums used in these experiments, the wall losses account for about 75% of the total energy lost (the remainder goes out through the LEHs; there are no capsule losses in these hohlraums). The observed 50% increase in the opacity of the composite could result in a 15% reduction in wall loss and in 12% less energy required to achieve the same hohlraum temperature. Alternatively, on Nova, the same amount of laser energy could lead to an increase in temperature of about 8 eV (about 12% more flux available to drive a capsule). The reduction in wall loss for the National Ignition Facility, the planned 1.8-MJ laser designed to achieve ignition in an ICF target, is even more dramatic. Here, for the point design ignition target,[19] the energy lost to the hohlraum wall would be reduced by about 160 kJ if the pure Au hohlraum was replaced with a hohlraum made of the 37% Au, 63% Gd composite. For an alternate ICF reactor based on a 10-MJ heavy-ion driver,[4] a reduction of 1.7 MJ in wall loss can be realized with the Au/Gd hohlraum wall.

Acknowledgments

We thank J. D. Kilkenny and B. Hammel for their support in conducting these experiments. We also acknowledge the Nova operations staff and target fabrication group for making these experiments possible.

Notes and References

1. Lindl, J. D., McCrory, R. L., and Campbell, E. M., *Physics Today,* **45** (9), p. 32–40 (1992).
2. Nuckolls, J. H., Wood, L., Thiessen, A. R., and Zimmerman, G. B., *Nature,* **239**, p. 139–142 (1972).
3. Lindl, J. D., *Physics of Plasmas,* **2**, p. 3933–4024 (1995).
4. Lindl, J. D., Bangerter, R. O., Mark, J. W.-K., and Pan, Y. L., "Review of Target Studies for Heavy Ion Fusion," *Heavy Ion Inertial Fusion*, M. Reiser, T. Godlove, and R. O. Bangerter, eds., *AIP Conf. Proc. 152* (American Institute of Physics, New York, 1986).
5. Rosen, M. D., "Scaling Law for Radiation Temperature," Lawrence Livermore National Laboratory, Livermore, CA, UCRL-50055-79, 1979 (unpublished).
6. Rosen, M. D., "Marshak Waves: Constant Flux vs. Constant T—a (slight) Paradigm Shift (U)," Lawrence Livermore National Laboratory, Livermore, CA, UCRL-ID 119548, 1995 (unpublished).
7. Pakula, R., and Sigel, R., *Phys. Fluids,* **28**, p. 232–244 (1985); **29**, p. 1340(E) (1986).
8. Marshak, R. E., *Phys. Fluids*, **1**, p. 24–29 (1958).
9. Rosseland, S., *Monthly Notices of the Royal Astronomical Society*, **84**, No 7 (1924).
10. Larsen, J. T., "Hyades—A Radiation Hydrodynamics Code for Dense Plasma Studies," *Radiative Properties of Hot Dense Matter: Proceedings of the 4th International Workshop*, W. Goldstein, C. Hooper, J. Gauthier, J. Seely, R. Lee, eds. (World Scientific, Singapore, 1990).
11. Nishimura, H., Endo, T., Shigara, H., Kato, Y., and Nakai, S., *Bull. Am. Phys. Soc.* **37**(6), p 1383 (1992). Also, *Appl. Phys. Lett.* **62**(12), p 1344 (1993).
12. Lokke, W. A., and Grasberger, W. H., "XSNQ-U, a non-LTE emission and absorption coefficient subroutine," Lawrence Livermore National Laboratory, Livermore, CA, UCRL-52276, 1977 (unpublished).
13. Sigel, R., et al., *Phys. Rev. Lett.*, **65**, p. 587–590 (1990).
14. Porter , J. L., and Thiessen, A. R., "Summary of albedo experiments," Lawrence Livermore National Laboratory, Livermore, CA, CLY-92-059, 1992 (unpublished).
15. White, V. J. L., Foster, J. M., Hansom, J. C. V., and Rosen, P. A., *Phys. Rev E* **49**, p. R4803–R4806 (1994).
16. Ze, F., Kania, D. R., Langer, S. H., Kornblum, H., Kauffman, R., Kilkenny, J., Campbell, E. M., and Tietbohl, G., *J. Appl. Phys.* **66**, p. 1935–1939, (1989).
17. Kauffman, R. L., Suter, L., Darrow, C. B., Kilkenny, J. D., Kornblum, H. N., Montgomery, D. S., Phillion, D. W., Rosen, M. D., Thiessen, A. R., Wallace, R. J., and Ze, F., *Phys. Rev Lett.* **73**, p. 2320–2323 (1994).
18. Kornblum, H. N., Kauffman, R. L., and Smith, J. A., *Rev. Sci. Instrum.* **57**, p. 2179–2181 (1986).
19. Haan, S. W., et al., *Phys. Plasmas* **2**, p. 2480–2486 (1995).